

Discovery of Novel Tubulin Inhibitors via Structure-Based Hierarchical Virtual Screening

Ran Cao,^{†,‡,⊥} Minyu Liu,^{§,||,⊥} Min Yin,[§] Quanhui Liu,^{||} Yanli Wang,^{*,‡} and Niu Huang^{*,‡}

[†]School of Pharmaceutical Science and Technology, Tianjin University, Tianjin 300072, China

[‡]National Institute of Biological Sciences, Beijing, No. 7 Science Park Road, Zhongguancun Life Science Park, Beijing 102206, China

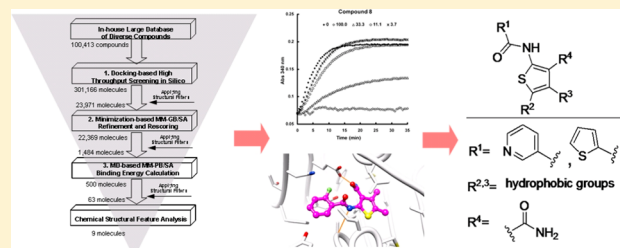
[§]School of Pharmacy, Shanghai Jiao Tong University, 800 Dong Chuan Road, Shanghai 200240, China

^{||}Department of Pharmacology, Shanghai Institute of Pharmaceutical Industry, 1111 Zhong Shan Bei Yi Road, Shanghai 200437, China

Supporting Information

ABSTRACT: To discover novel tubulin inhibitors, we performed structure-based virtual screening against the colchicine binding pocket. In combination with a hierarchical docking and scoring procedure, the structural information of an additional subpocket in colchicine site was applied to filter out the undesired docking hits. This strategy automatically resulted in 63 candidates meeting the structural and energetic criteria from a screening library containing approximately 100 000 diverse druglike compounds. Among them, nine molecules were chosen for experimental validation, which all share the similar binding

pose and contain an enriched scaffold bearing thiophene core. Encouragingly, five compounds are active in tubulin polymerization assay. The most potent inhibitor, 2-(2-fluorobenzamido)-3-carboxamide-4,5-dimethylthiophene, is structurally distinct to any known colchicine site binders and has higher ligand efficiency than colchicine. On the basis of its predicted binding pose, we systematically probed its binding characteristics by testing series of structural modifications. The obtained structure–activity relationship results are consistent with our binding model, and the inhibition activities of two analogues are improved by 2-fold. We expect that the novel structure discovered in the present study may serve as a starting point for developing tubulin inhibitors with improved efficacy and fewer side effects. We also expect that our hierarchical strategy may be generally applicable in structure-based virtual screening campaigns.



INTRODUCTION

Microtubules are critical for the function of eukaryotic cells, including the formation of cytoskeleton and spindle, which play essential roles in cellular architecture maintenance and chromosome segregation.¹ Because of their crucial role in mitotic events, microtubules serve as important drug targets for anticancer chemotherapy. Microtubules are long filamentous and tube-shaped protein polymers that are composed of α - and β -tubulin heterodimers with a head-to-tail association.² There are three well-characterized ligand binding sites (Figure 1A): vinca site at the interface between α - and β -subunits of different tubulin heterodimers, taxol site at the surface in the lower part of the β -subunit, and colchicine site at the interface between the α - and β -subunits of the same tubulin heterodimer.^{3,4} Antimitotic drugs targeting the vinca and taxol sites such as Vinblastine and Taxol have been applied in the clinical treatment of a wide range of tumors.^{1,3,5} However, their clinical usages have been hampered by the multiple drug resistance (MDR) and numerous adverse effects such as neurotoxicity.⁶

Colchicine site inhibitors are less structurally complicated than taxol and vinca site binders (Figure 1B), and might hold

the promise to developing novel antimitotic drugs with better properties.⁷ For example, colchicine site binder E7010 was found to overcome MDR on numerous tumor cell lines.⁸ Another colchicine site binder, indibulin, was reported to be effective toward MDR tumor cells as well as lack of neurotoxicity.^{9,10} In addition, several colchicine site microtubule inhibitors were found to act as the vascular disrupting agents (VDA), besides their antimitotic activity.^{11,12} 2-Methoxyestradiol was shown to inhibit angiogenesis, and combretastatin A-4 (CA4) and its prodrug (CA4P) were reported to disrupt tumor blood flow with lack of toxicity on normal vasculature.^{13,14} These results have inspired interest in searching for novel colchicine site ligands with improved anticancer potency and less side effects.^{15–18}

State-of-the-art virtual screening techniques have been established as invaluable tools to narrow the size of the screening compound library to the most promising drug candidates.^{19,20} There are two broad categories, ligand-based methods and structure-based approaches. Ligand-based ap-

Received: June 29, 2012

Published: September 20, 2012



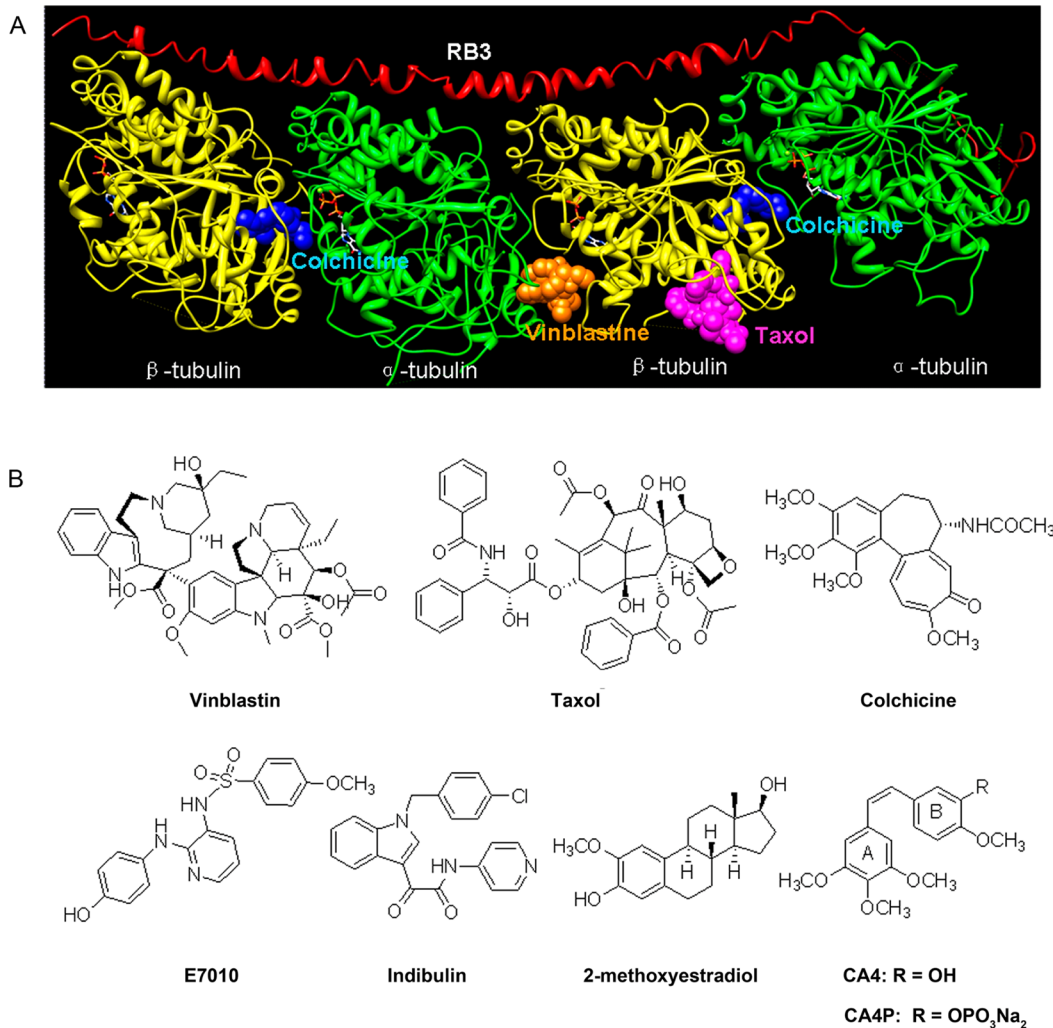


Figure 1. (A) Three distinct ligand binding sites located on tubulin. Crystal structures of tubulin bound with vinblastine and colchicine (PDB ID: 3E22), and taxol (PDB ID: 1JFF) are superimposed. For clarity, only colchicine bound tubulin structure is shown with the presence of all three ligands. α -Tubulin, β -tubulin, and RB3 are colored in green, yellow, and red ribbon, respectively. Vinblastine and colchicine are represented by orange and blue space-filling models, GTP and GDP are represented by orange stick, and taxol is shown in magenta space-filling representation. Graphic images were prepared with Chimera. (B) Chemical structures of antitubulin agents.

proaches (e.g., pharmacophore search) rely on a series of active compounds to derive the structural features for describing certain biological activities and were applied in the discovery of colchicine site antitubulin agents.^{21,22} In contrast, target structure-based methods (e.g., molecular docking) generally only require the experimental structure of a known target to navigate the receptor–ligand binding space and have the advantage of finding the first lead of new targets without depending on any information of known ligands. Surprisingly, the number of tubulin–inhibitor complexes has increased rapidly; however, there are very few reports on discovering novel tubulin inhibitors using structure-based virtual screening methods. Nguyen et al. developed a common pharmacophore for a diverse set of colchicine site inhibitors using docking and molecular dynamics (MD) simulation, which was further assessed by Massarotti et al. in exploring new inhibitors.^{23,24}

Noteworthy, the recently published crystal complex structure of tubulin bound with a novel inhibitor, NSC613863 (the chiral *R* isomer of ethyl-5-amino-2-methyl-1,2-dihydro-3-phenylpyrido[3,4-*b*]pyrazin-7-yl-carbamate), revealed that the ligand induces conformational change in the colchicine site and

occupies a deeply buried subpocket (designated as additional pocket).² This was also observed in another complex structure bound with ligand TN16.²⁵ NSC613863 was shown to be more potent than colchicine in both molecular and cellular antipolymerization assays.^{26–28} Interestingly, before the crystal complex structures bound with NSC613863 and TN16 were reported, this additional pocket was predicted by Kim et al. in their binding model of ligand MDL-27048, a microtubules destabilizing agent.²⁹ Here, we were wondering whether it is possible to identify an extremely different tubulin inhibitor via virtual screening of a large database by targeting this additional pocket in colchicine site, and to predict its binding pose correctly.

RESULTS AND DISCUSSION

Binding Site Analysis. To discover novel tubulin inhibitors, the crystal structure of tubulin bound with NSC613863 (PDB ID: 3N2G) was used for docking screening. NSC613863 occupies different space in the binding pocket as compared to colchicine (Figure 2A and B). Upon NSC613863 binding, an enlarged pocket is induced with α -helix H8 drifting

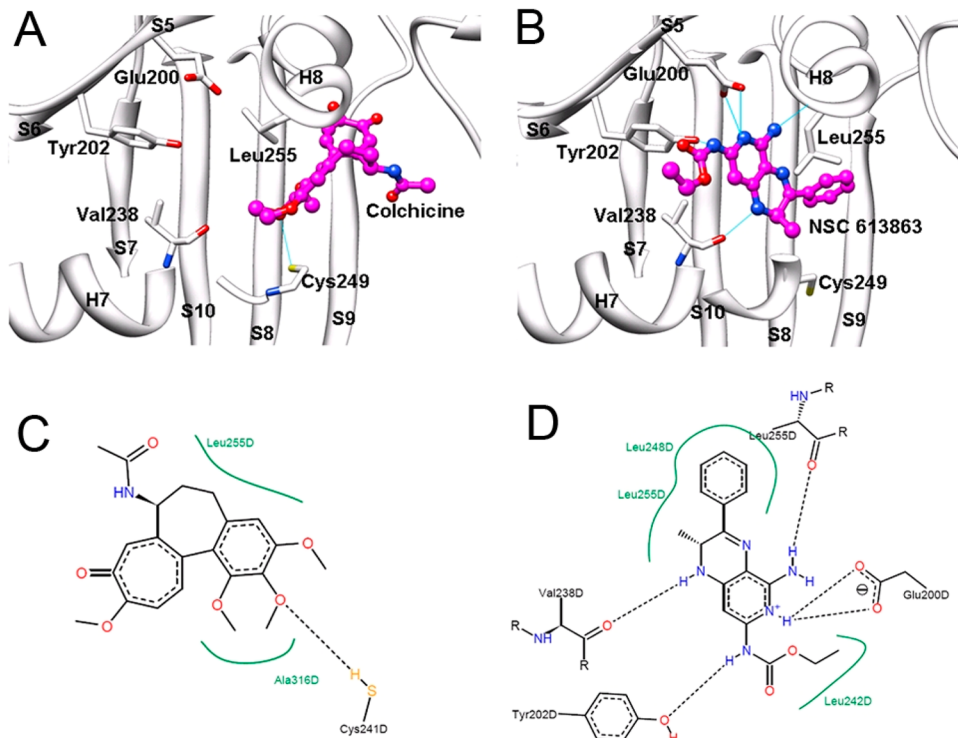


Figure 2. (A) Binding mode of colchicine (magenta, ball and stick) in context of β -tubulin (white, ribbon); the hydrogen bond between colchicine and residue Cys249 is illustrated as a cyan line. The side chain of Leu255 is in a flip-in conformation. (B) Binding mode of NSC613863 (magenta, ball and stick) in context of β -tubulin (white, ribbon); hydrogen bonds between NSC613863 and residues Glu200, Tyr202, Val238, and Leu255 are illustrated in cyan lines. The side chain of Leu255 is in a flip-out conformation. (C,D) Schematic diagrams of binding modes of colchicine and NSC613863, generated using PoseView software (<http://www.poseview.de/poseview>).

away from β -sheet S8–S10,² and the side chain of Leu255 locating at H8 flips out in comparison with the flip-in conformation in the apo state (PDB ID: 3HKB)²⁵ and in colchicine bound complex structure, with a large root-mean-square deviation (rmsd) value of 3.74 Å (Table S1 in the Supporting Information). Therefore, the flipped out Leu255 opens a deeply buried subpocket to accommodate NSC613863, and several favorable polar interactions are forming between NSC613863 and residues belonging to β strands S5 and S6 in the N-terminal nucleotide-binding domain (Figure 2C and D).^{2,30} This structural phenomenon was also observed in the TN16 bound complex structure, which occupies the same space as NSC613863.

On the basis of these detailed binding site analyses, we defined three structural filters to remove undesired docking hits. First, the ligands shall be accommodated in the Leu255 flip-out conformation, and thus shall generate steric clashes with the side-chain atoms of Leu255 in flip-in conformation. Second, the qualified ligands shall form close atomic contacts (i.e., distance cutoff of 4 Å) with hydrophobic residues in the additional pocket, including Tyr52, Phe169, Tyr202, Val238, and Leu242. Third, the desired candidates shall form at least one hydrogen-bond interaction (i.e., distance threshold of 4 Å) with polar atoms in the additional pocket as does NSC613863, including the oxygen atom of hydroxyl group in Tyr202, the oxygen atom of carbonyl groups in Leu255 and Val238, and the oxygen atoms of carboxyl group of Glu200.

Structure-Based Virtual Screening. To strike the balance of efficiency and accuracy, we developed a hierarchical strategy to integrate different computational methods in an increasing order of complexity and more physically realistic manner

(Figure 3). Briefly, our hierarchical procedure consists of three steps: (1) Predicting the binding poses of ligands using a fast-compute docking program;^{31–33} (2) optimizing and rescoring the docked ligand in protein binding pocket using molecular-mechanics (MM) force field in combination with generalized

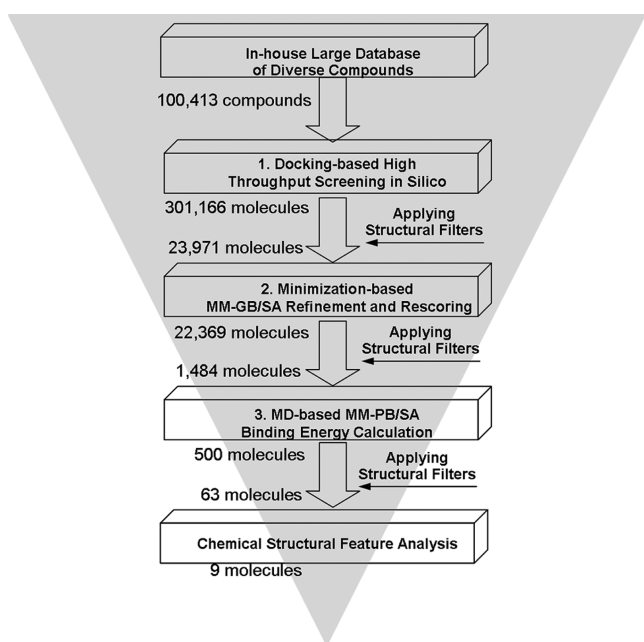


Figure 3. Flowchart of our structure-based hierarchical virtual screening strategy.

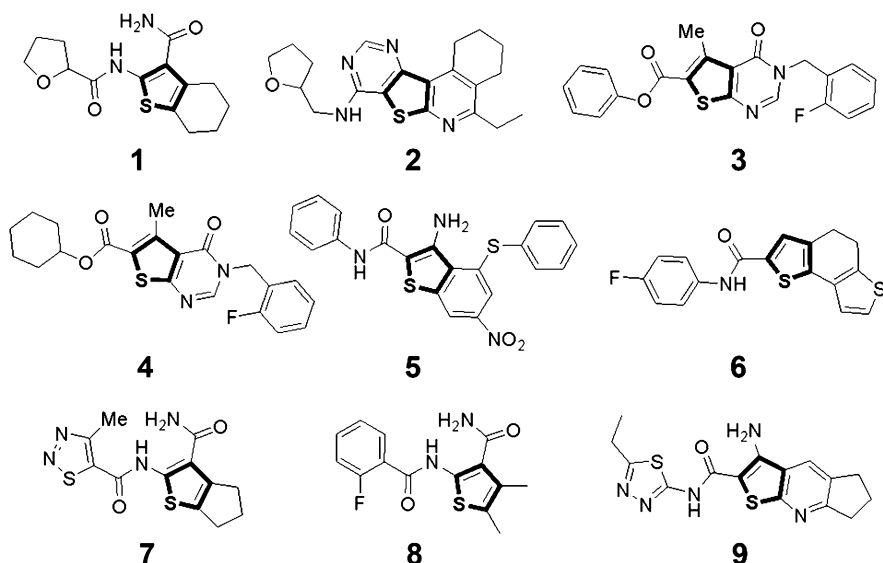


Figure 4. Chemical structures of nine candidates bearing thiophene core (highlighted with bold line).

born surface area (GB/SA) implicit solvent;^{34–37} and (3) running molecular dynamics (MD) simulations on the top scoring complex in explicit water, and the ligand binding free energy is estimated by ensemble averaging the gas-phase enthalpy and solvation free energy using the molecular-mechanics Poisson–Boltzmann surface area (MM-PB/SA) method.³⁸ Note that the predefined structural filters were applied to eliminate the undesired hits after each step of ranking and scoring, and the hydrogen-bond interaction was defined using more stringent criteria in analyzing MM-GB/SA and MM-PB/SA results (i.e., distance threshold of 3.5 Å). We expect that such hierarchical protocol can maximally reduce the false positives produced by the limited sampling and deficient scoring function.

We first docked our in-house compound library containing 100 000 diverse druglike compounds and generated more than 300 000 binding poses. This step only takes on average 0.1 s per compound on a single CPU core. After the docking poses unsatisfying the structural filters were removed, 23 971 nonredundant compounds were subjected to minimization-based MM-GB/SA refining and rescoring. The minimization procedure allows the docked molecule to optimize its interaction with binding-site residues and only takes less than 1 min on a single CPU core to process one protein–ligand complex. At this stage, the majority of molecules changed their initial docked geometries, and many drifted away from the additional pocket after minimization. Only 1484 hits passed the structural filters. We carried out 5 ns MD simulations for the top 500 MM-GB/SA scored hits to simultaneously sample the ligand along with the binding-site residues in the explicit water environment, taking approximately a day per complex on an eight-core CPU. Only 63 molecules were still satisfying the structural filters after this stage and were subjected for further visual examination. Interestingly, a thiophene scaffold is enriched among 15 molecules, nine of them (Figure 4) adopt similar binding pose with sulfur atom pointing toward Val238 in H7 α-helix. Note that the thiophene derivative has been reported as potent scaffold for tubulin inhibitor, including either benzothiophene core or thiophene substituted with trimethoxyphenyl group.^{39–43} However, our selected candidate compounds are structurally distinct with any of these known

thiophene-containing colchicine site binders, with calculated Tanimoto coefficients less than 0.3 (Table S2 in the Supporting Information).

Antimicrotubules Activity Assays. The turbidimetric method was performed on these nine chosen molecules at a concentration of 100 μM in the presence of Triton X-100 to prevent the nonspecific inhibition due to aggregation.⁴⁴ We used microtubules destabilizing agent colchicine as a positive control at the concentration of 8 μM. As compared to the DMSO control, five compounds (2, 3, 5, 7, and 8) show significant inhibition of the tubulin polymerization (Figure 5A), which strongly support a common mode of action shared by this series of compounds. Among these five actives, compound 8, 2-(2-fluorobenzamido)-3-carboxamide-4,5-dimethylthiophene, is the most potent one at 50 μM (Figure 5B). To further confirm its activity, we carried out the sedimentation assay. Both microtubules stabilizing and destabilizing agents, colchicine and taxol, were used as our controls. In this assay, the amount of tubulin in the supernatant was largely reduced in the reacting sample incubated at 37 °C as compared to sample maintained at 0 °C, which suggests the formation of microtubules. 50 μM compound 8 (Figure 6A) can significantly increase the amount of unassembled tubulin in the supernatant at 37 °C (Figure 6B), consistent with turbidimetric assay results. Colchicine strongly destabilizes microtubules at 20 μM, while taxol is shown to have a polymerization promoting effect at 5 μM by retaining little tubulin content in the supernatant.

Accurately ranking and scoring a library of diverse compounds is still challenging; therefore, a simple yet effective way to improve the hit rate in virtual screening application is to exclude molecules forbidden from the essential structural criteria.^{45,46} Here, we did not sorely rely on the energy scores to select the compounds for experimental testing. Instead, we applied a hierarchical strategy to reduce the size of screening database step wisely, until dozens of compounds having favorable binding energies and reasonable binding modes satisfy the predefined structural filters. Surprisingly, such simple component is sufficient to get reasonable results. Especially the most potent compound, compound 8, would not be discovered whatsoever based on any of these calculated energy scores (Table S3 in the Supporting Information). We expect that such

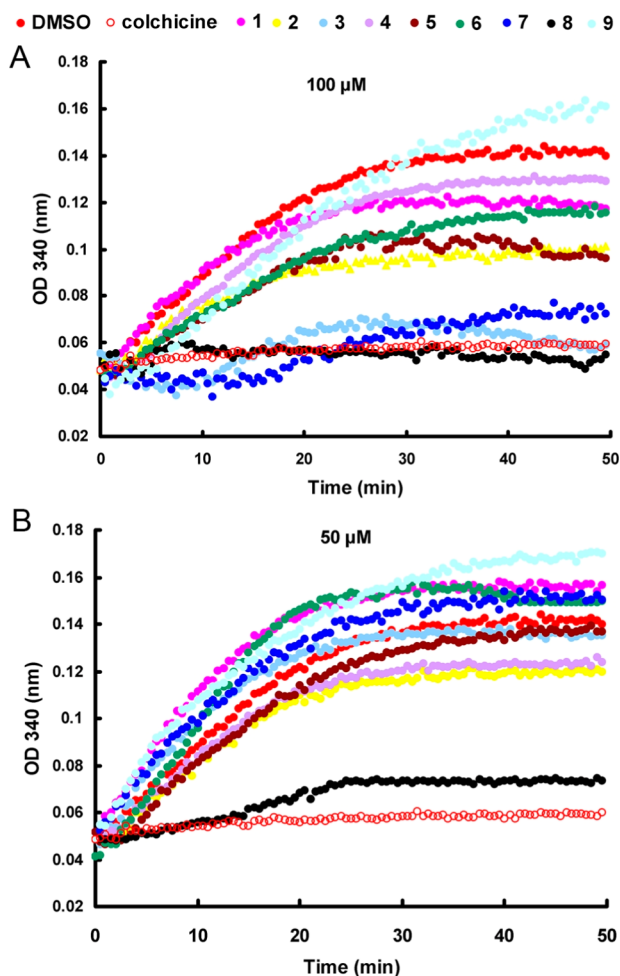


Figure 5. Antipolymerization potency of nine candidates tested at concentrations of (A) 100 μM and (B) 50 μM determined with turbidimetric assay.

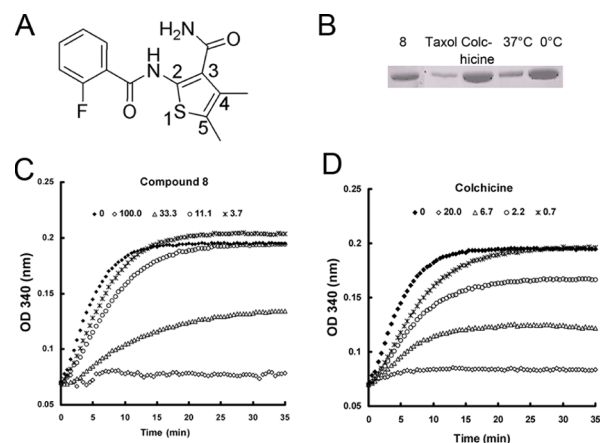


Figure 6. (A) Chemical structure of lead compound 8. (B) Antipolymerization potency of compound 8 determined by sedimentation assay at 50 μM . (C,D) Dose response antipolymerization activity of compound 8 and colchicine determined by turbidimetric assay, respectively. The IC₅₀ values were determined for compound 8 ($30 \pm 5 \mu\text{M}$) and colchicine ($5 \pm 1 \mu\text{M}$) from three independent tests.

strategy may have general usage in structure-based virtual screening practices.

We further determined the dose response inhibition activity of 8 using turbidimetric assay, and the IC₅₀ (50% inhibition of microtubules formation) value was determined from three independent tests and reported as mean \pm SD μM . The determined IC₅₀ value of compound 8 is $30 \pm 5 \mu\text{M}$ (Figure 6C). At the same assay condition, colchicine shows stronger potency with an IC₅₀ value of $5 \pm 1 \mu\text{M}$ (Figure 6D), consistent with a previously reported value (IC₅₀ = 6 μM).⁴⁷ Although the inhibition activity of compound 8 is 6-fold less potent than colchicine, it has higher ligand efficiency^{48,49} than colchicine, about 1.2-fold more efficient. This indicates that compound 8 may serve as a good starting point for further lead optimization. The microtubules inhibition effect of compound 8 was also studied with rhodamine-labeled tubulin using confocal microscopy technique. Similar to colchicine, compound 8 can significantly inhibit the tubulin polymerization at 50 μM (Supporting Information Figure S1).

Validation of Predicted Binding Mode. Compound 8 represents a novel class of tubulin inhibitors. On the basis of its predicted binding mode and the potential chemical modifications, we probed the binding characteristics by proposing and testing series of structural analogues. According to our prediction, 8 is deeply buried in the inner part of the colchicine binding pocket with 2-(2-fluorobenzamido) group inserting into the additional pocket while two methyl substituents point toward the interface of α - and β -tubulin heterodimer (Figure 7A).

First, we focused on the R¹-substituent on the phenyl group where the space is relatively enclosed and limited without permitting large modifications (Figure 7B). Specifically, the ortho-position is surrounded by residues Asn167, Glu200, and Tyr202, and only allows small substitutes such as fluorine atom (8) and hydrogen atom (8-f). This is validated by gradually decreased potencies for larger substituents, such as chlorine (8-a), bromine (8-b), and iodine (8-c) (Table 1). Similarly, the meta- and para-positions consist of residues Tyr52, Gln136, Asn167, Phe169, and Tyr202 located at H7 α -helix and S5, S6, S7 β -sheets, allowing limited space for potential substituents. Both positions are against nonpolar atoms, including phenyl group of Phe169, C β of Gln136 and Asn167, which suggests polar groups at these sites are unfavorable. This is consistent with the loss of activity of both *meta*- and *para*-fluorine substituents (8-d and 8-e). The aromatic and hydrophobic residues around R¹ substituent indicate the requirement of similar properties. This is supported from the observation that aromatic rings (8-f, 8-g, and 8-i) are active, while saturated groups (8-h and 8-j) lose activity. In addition, there are also polar residues around this position, such as the hydroxyl group of Tyr52 and amine group of Gln136, pointing toward the 3'-site of phenyl group. This suggests a potential hydrogen-bond acceptor at 3'-site would improve the ligand potency. Remarkably, this hypothesis is confirmed by 2-fold improvement of both 3'-pyridine (8-g) and 2'-thiophene (8-i) rings as compared to the benzene group (8-f).

For R²- and R³-substituents, the surrounding environment is relatively large and tolerable for bulky groups (Figure 7C). Specifically, the 4,5-dimethyl groups extend outside toward the interface of α - and β -tubulin heterodimer consisting of side chains of hydrophobic residues Leu248, Leu255, Val318, Ala316, and Ile378, which suggests hydrophobic substituents would be preferred. We chose compound 8-i as a reference compound for this series of modifications due to the commercial availability (Table 2). It is evident that diverse

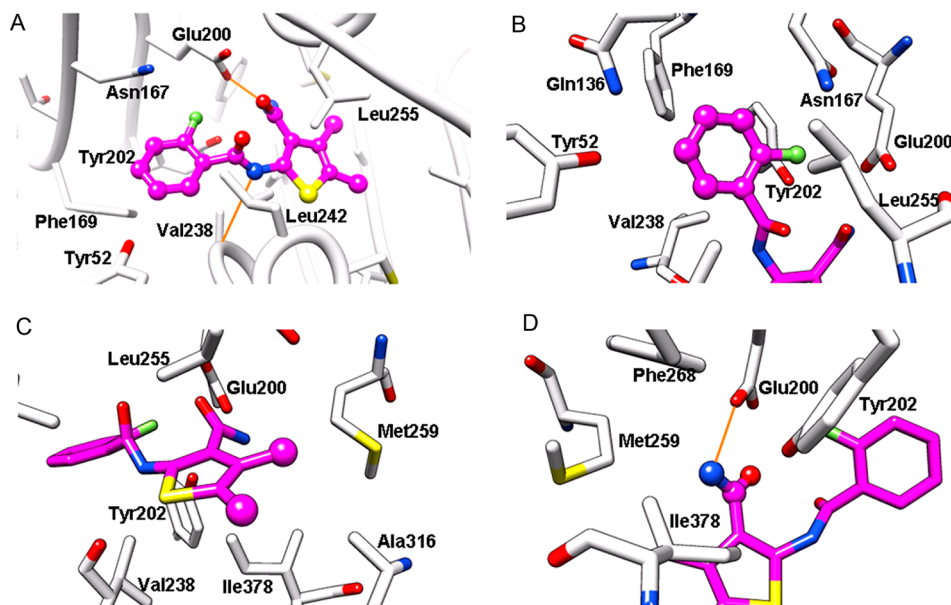


Figure 7. (A) Overall view of predicted binding model of compound 8 (magenta, ball and stick). (B) Focused view of R^1 group (ball and stick) in context of surrounding residues (white, stick). (C) Focused view of R^2 and R^3 groups (ball and stick) in context of surrounding residues (white, stick). (D) Focused view of R^4 group (ball and stick) in context of surrounding residues (white, stick).

Table 1. SAR of Modifications of R^1 Substituent^a

No.	R^1	IC_{50} (μM)	No.	R^1	IC_{50} (μM)
8		30 ± 5	8-a		40 ± 5
8-b		50 ± 4	8-c		>100
8-d		>100	8-e		>100
8-f		35 ± 5	8-g		16 ± 3
8-h		>100	8-i		14 ± 2
8-j		>100			

^a IC_{50} values were determined for each compound (mean \pm SD μM) from three independent tests.

Table 2. SAR of Modifications of Both R² and R³ Substituents^a

No.	R ²	R ³	IC ₅₀ (μM)
8-i	CH ₃	CH ₃	14 ± 2
8-k			35 ± 3
8-l			32 ± 1
8-m			22 ± 1
8-n		CH ₃	45 ± 3
8-o	CH ₃		23 ± 3

^aIC₅₀ values were determined for each compound (mean ± SD μM) from three independent tests.

substituents at this position do not change the potency largely (IC₅₀ values from 22 to 45 μM), including both saturated groups (**8-k**, **8-l**, and **8-m**) and aromatic groups (**8-n** and **8-o**). This agrees with our prediction that the bulky groups are tolerant at this position.

For the R⁴-substituent, the 3-carboxamide moiety points against Glu200 of H8 α-helix and is surrounded by Tyr202, Met259, and Phe268 (Figure 7D), which makes negative-charged substituent intolerable and the bulky group unfavorable. In comparison, groups with a hydrogen donor such as amine in compound **8** would be expected to contribute to the binding affinity, while loss of this interaction would decrease the potency. As we expected, the substitution of amine with carboxyl group (**8-p**, **8-q**, and **8-r**) sacrificed the binding affinity with IC₅₀ > 100 μM (Table 3), which is consistent with the existence of negative-charged residue Glu200 nearby. The substitutions with bulky groups, such as hydrazine (**8-s**), morpholine (**8-u**), and 4-chlorobenzenamine (**8-v**), all sacrificed the potency strongly, which confirms the critical requirement for the space at this position. In addition, the decreasing of potency for methyl substituent (**8-t**) supports our hypothesis that the hydrogen bond between the carboxyl group of Glu200 and the amine group of ligand is important to the activity of lead compound **8**.

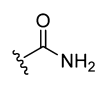
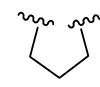
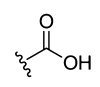
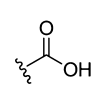
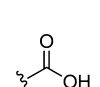
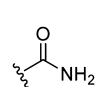
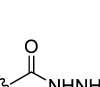
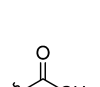
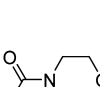
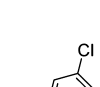
On the basis of our SAR studies on compound **8**, we can easily interpret the results of our initial screened nine candidate

compounds. Clearly, compound **1** is inactive because the R¹ subsite prefers the aromatic phenyl ring over the aliphatic furan group (Table 1). Similarly, the lack of activity of compounds **4** and **9** may be caused by the intolerable bulky groups at the R¹ subsite, such as the saturated cyclohexane ring and the ethyl substituent on the aromatic ring, respectively. Nevertheless, a further SAR exploration structural biology study on compound **8** will be pursued.

CONCLUSION

In the present study, we performed structure-based virtual screening against colchicine binding site. To strike the balance of the computational cost and prediction efficiency, we employed a hierarchical strategy to integrate different computational methods in an increasing order of complexity and more physically realistic manner. This strategy relies on the assumption that the ligand binding poses can be effectively predicted using approximate docking approaches. Thus, a fast-compute docking method was applied to generate docking poses, followed by the refinement and rescore using the minimization-based MM-GB/SA method in implicit solvent model. Finally, the molecular dynamics-based MM-PB/SA was employed to take account of the binding-site flexibility in water environment. Postprocessing of molecular docking poses using more rigorous physics-based methods has become more frequently carried out in virtual screening campaigns; however,

Table 3. SAR of Modifications of R¹, R², R³, and R⁴ Substituents^a

No.	R ¹	R ²	R ³	R ⁴	IC ₅₀ (μM)
8		CH ₃	CH ₃		30 ± 5
8-p					>100
8-q					>100
8-r					>100
8-f		CH ₃	CH ₃		35 ± 5
8-s		CH ₃	CH ₃		>100
8-t					>100
8-u					>100
8-v					>100

^aIC₅₀ values were determined for each compound (mean ± SD μM) from three independent tests.

accurately ranking and scoring a library of diverse compounds is still challenging. In the present study, we incorporate the information of protein–ligand binding characteristics into virtual screening by filtering out the undesired hits after each step of ranking and scoring, and this simple component is sufficient to get reasonable results. Encouragingly, five out of nine molecules chosen from 100 000 screening compounds have shown tubulin inhibitory activity. The most potent inhibitor, compound **8**, is structurally distinct from any

known colchicine site binders. Its potency was validated with different tubulin polymerization assays. On the basis of the binding prediction, we designed a series of structural modifications. The obtained SAR results strongly support our predicted binding pose and lead to more potent inhibitors. Because of the high ligand efficiency of our identified lead compounds, we expect that our current work serves as a starting point to develop novel tubulin inhibitors with improving efficacy and fewer side effects.

MATERIALS AND METHODS

Our internal screening compound library was constructed from the ChemDiv commercially available compound database (<http://eu.chemdiv.com>) by maximizing the structural diversity. The new series of compounds designed for SAR studies were purchased from ChemBridge (<http://www.chembridge.com>) and Vitas-M Lab library (<http://www.vitasmlab.com>), respectively. The vendors had verified the compound purity by liquid chromatography–mass spectrometry (LC–MS) or nuclear magnetic resonance (NMR) experiments. The ¹H NMR spectrum and MS data for identified active compounds 8, 8-g, and 8-i are included in the Supporting Information (Figures S2–7) to further validate their structure and purity.

For computational screening, we used crystal structure of α,β -tubulin heterodimer complex with ligand NSC613863 (PDB ID: 3N2G) as our receptor model after deleting all solvents and cofactors. Docking was performed with DOCK 3.5.54, a flexible-ligand method that uses a force-field-based scoring function composed of van der Waals and electrostatic interaction energies corrected for ligand desolvation.^{31–33} All of the compounds in the library were prepared in db format with ZINC protocol.⁵⁰ Binding site residues were identified within 12 Å of NSC613863, and the solvent-accessible molecular surface⁵¹ was calculated with the program DMS⁵² using a probe radius of 1.4 Å. Receptor-derived spheres were generated with the program SPHGEN,⁵³ while the ligand-derived spheres were from the positions of the heavy atoms of NSC613863. Four sets of grids were generated: an excluded volume grid using DISTMAP,³¹ a united atom AMBER-based van der Waals potential grid using CHEMGRID,³¹ an electrostatic potential grid using DelPhi,⁵⁴ and a solvent occlusion map using the program SOLVMAP.⁵⁵ Ligand conformations were scored on the basis of the total energy after 25 steps of rigid-body minimization, which is the sum of electrostatic and van der Waals interaction energies, corrected by the partial ligand desolvation energy.

MM-GB/SA refinement and rescoring was performed using the Protein Local Optimization Program (PLOP).^{34–36} This approach accounts for more accurate and efficient calculations of ligand–protein interaction energies, the ligand/receptor desolvation, and, to a lesser extent, ligand strain energies. Briefly, the docked protein–ligand complex and ligand were submitted to multiscale Truncated Newton energy minimization in all-atom OPLS force field and Generalized Born solvent as described previously.^{37,56,57} The protein structure used in the docking was used for rescoring. Hydrogen atoms were added in standard geometries as defined by the all-atom OPLS force field.^{58,59} The protein was kept rigid during ligand–protein complex minimization in this work. The binding energy ($E_{\text{bind}} = E^{\text{R*L}} - E^{\text{L}} - E^{\text{R}}$) was calculated by subtracting the energies of the optimized free ligand in solution (E^{L}) and the free protein in solution (E^{R}) from the optimized ligand–protein complex's energy in solution ($E^{\text{R*L}}$).

MM-PB/SA calculation was carried out using AMBER10.0 suite.⁶⁰ AMBER99SB force field⁶¹ was applied for receptor, and the general Amber force field (GAFF)⁶² was applied for the ligands. ANTECHAMBER was used for calculating the AM1-BCC charges of ligands. All system setups were performed in TLEAP module. Simulations were carried out using SANDER module. For each complex, three stages of minimization were performed in the gas phase, followed by the addition of a 30 Å water cap based on the geometric center of binding site. After

200 ps of equilibration of solvents, a production run of 5 ns was performed on the whole system at 300 K with a time step of 2.0 fs. All residues including solvents beyond 12 Å of ligand are fully frozen. 100 snapshots were evenly extracted from last 1 ns simulation. The interaction energy between receptor and ligand as well as the internal energy were calculated with the SANDER module. As for the solvation energy, the polar contribution is calculated using PBSA⁶³ with PARSE radii, while the nonpolar part is estimated proportional to the solvent-accessible surface area.⁶⁴ All of the computational tasks were performed on our Linux clusters and managed with the scheduling system SGE.

Porcine brain tubulin was purified as described previously.⁶⁵ Briefly, after being purified by two cycles of polymerization–depolymerization in a high-molarity buffer, porcine brain tubulin was assembled in 80 mM PIPES-K (pH 6.9) (containing 1 mM EGTA, 1 mM MgCl₂, 30% glycerol) and disassembled and stored in buffer PIPES-K (pH 6.9) (containing 1 mM EGTA, 1 mM MgCl₂).

Sedimentation experiment was carried out as described previously.⁶⁶ Briefly, 19 μL of 2 mg/mL ice-cold porcine brain tubulin solution (in 80 mM PIPES-K, pH 6.9, 0.5 mM MgCl₂, 1 mM EGTA, 5 mM GTP, and 10% glycerol) was mixed with 1 μL of DMSO or 1 μL of compound solution in DMSO. The mixture was incubated at 37 °C for 15 min, and 20 μL of the mixture was loaded on a 30 μL of glycerol cushion (80 mM PIPES-K, pH 6.9, 0.5 mM MgCl₂, 1 mM EGTA, 5 mM GTP, and 50% glycerol) pre-equilibrated at 37 °C. The mixture was spun for 5 min at 75 000 rpm at 37 °C. Proteins in the supernatant were analyzed by SDS-PAGE.

Turbidimetric assay was carried out as described previously.⁶⁶ 99 μL of ice-cold porcine brain tubulin (2 mg/mL) (in 80 mM PIPES-K, pH 6.9, 1 mM MgCl₂, 0.5 mM EGTA, 3 mM GTP, and 15% glycerol) was mixed with 1 μL of DMSO or compound solution in DMSO. The mixture was immediately transferred to a 96-well plate equilibrated at 37 °C. Changes in the OD at 340 nm were monitored every 30 s with a Beckman Coulter Paradigm Detection Platform at 37 °C.

ASSOCIATED CONTENT

Supporting Information

Antipolymerization effects of colchicine and compound 8 using confocal microscopy, and the ¹H NMR spectrum and MS data of the three active compounds 8, 8-g, and 8-i. The rmsd values of the residues in additional pocket upon NSC613863 binding, structural similarity analysis between lead compound 8 and representative tubulin inhibitors, and energy scores of nine originally selected candidates. This material is available free of charge via the Internet at <http://pubs.acs.org>.

AUTHOR INFORMATION

Corresponding Author

*Phone: 86-10-80720645 (N.H.); 86-10-80726688-8573 (Y.W.). Fax: 86-10-80720813 (N.H.); 86-10-80720813 (Y.W.). E-mail: huangniu@nibs.ac.cn (N.H.); wangyanli@nibs.ac.cn (Y.W.).

Author Contributions

[†]These authors contributed equally.

Notes

The authors declare no competing financial interest.

ACKNOWLEDGMENTS

We are grateful for financial support from the Chinese Ministry of Science and Technology "973" Grant 2011CB812402 (to N.H.). We thank Fanqi Zeng for helping with spectrum analysis. We also thank Wei Shao and Dr. Xiaoguang Lei for providing compounds from the NIBS compound collection. Computational support was provided by the Supercomputing Center of Chinese Academy of Sciences (SCCAS) and the Beijing Computing Center (BCC).

ABBREVIATIONS

MDR, multiple drug resistance; VDA, vascular disrupting agents; MD, molecular dynamics; rmsd, root-mean-square deviation; MM, molecular-mechanics; GB/SA, generalized born surface area; MM-PB/SA, molecular-mechanics Poisson–Boltzmann surface area; LC–MS, liquid chromatography–mass spectrometry; NMR, nuclear magnetic resonance; PLOP, Protein Local Optimization Program; GAFF, general Amber force field; SAR, structure–activity relationship

REFERENCES

- (1) Jordan, M. A.; Wilson, L. Microtubules as a target for anticancer drugs. *Nat. Rev. Cancer* **2004**, *4*, 253–265.
- (2) Barbier, P.; Dorleans, A.; Devred, F.; Sanz, L.; Allegro, D.; Alfonso, C.; Knossow, M.; Peyrot, V.; Andreu, J. M. Stathmin and interfacial microtubule inhibitors recognize a naturally curved conformation of tubulin dimers. *J. Biol. Chem.* **2010**, *285*, 31672–31681.
- (3) Schmidt, M.; Bastians, H. Mitotic drug targets and the development of novel anti-mitotic anticancer drugs. *Drug Resist. Updates* **2007**, *10*, 162–181.
- (4) Massarotti, A.; Coluccia, A.; Silvestri, R.; Sorba, G.; Brancale, A. The tubulin colchicine domain: a molecular modeling perspective. *ChemMedChem* **2012**, *7*, 33–42.
- (5) Singh, P.; Rathinasamy, K.; Mohan, R.; Panda, D. Microtubule assembly dynamics: an attractive target for anticancer drugs. *IUBMB Life* **2008**, *60*, 368–375.
- (6) Kavallaris, M. Microtubules and resistance to tubulin-binding agents. *Nat. Rev. Cancer* **2010**, *10*, 194–204.
- (7) Risinger, A. L.; Giles, F. J.; Mooberry, S. L. Microtubule dynamics as a target in oncology. *Cancer Treat. Rev.* **2009**, *35*, 255–261.
- (8) Yoshimatsu, K.; Yamaguchi, A.; Yoshino, H.; Koyanagi, N.; Kitoh, K. Mechanism of action of E7010, an orally active sulfonamide antitumor agent: inhibition of mitosis by binding to the colchicine site of tubulin. *Cancer Res.* **1997**, *57*, 3208–3213.
- (9) Bacher, G.; Nickel, B.; Emig, P.; Vanhoefer, U.; Seeber, S.; Shandra, A.; Klenner, T.; Beckers, T. D-24851, a novel synthetic microtubule inhibitor, exerts curative antitumoral activity *in vivo*, shows efficacy toward multidrug-resistant tumor cells, and lacks neurotoxicity. *Cancer Res.* **2001**, *61*, 392–399.
- (10) Wienecke, A.; Bacher, G. Indibulin, a novel microtubule inhibitor, discriminates between mature neuronal and nonneuronal tubulin. *Cancer Res.* **2009**, *69*, 171–177.
- (11) Tozer, G. M.; Kanthou, C.; Baguley, B. C. Disrupting tumour blood vessels. *Nat. Rev. Cancer* **2005**, *5*, 423–435.
- (12) Kanthou, C.; Tozer, G. M. Microtubule depolymerizing vascular disrupting agents: novel therapeutic agents for oncology and other pathologies. *Int. J. Exp. Pathol.* **2009**, *90*, 284–294.
- (13) D'Amato, R. J.; Lin, C. M.; Flynn, E.; Folkman, J.; Hamel, E. 2-Methoxyestradiol, an endogenous mammalian metabolite, inhibits tubulin polymerization by interacting at the colchicine site. *Proc. Natl. Acad. Sci. U.S.A.* **1994**, *91*, 3964–3968.
- (14) Dumontet, C.; Jordan, M. A. Microtubule-binding agents: a dynamic field of cancer therapeutics. *Nat. Rev. Drug Discovery* **2010**, *9*, 790–803.
- (15) Chen, J.; Liu, T.; Dong, X.; Hu, Y. Recent development and SAR analysis of colchicine binding site inhibitors. *Mini-Rev. Med. Chem.* **2009**, *9*, 1174–1190.
- (16) Hsieh, H. P.; Liou, J. P.; Mahindroo, N. Pharmaceutical design of antimitotic agents based on combretastatins. *Curr. Pharm. Des.* **2005**, *11*, 1655–1677.
- (17) Tron, G. C.; Pirali, T.; Sorba, G.; Pagliai, F.; Busacca, S.; Genazzani, A. A. Medicinal chemistry of combretastatin A4: present and future directions. *J. Med. Chem.* **2006**, *49*, 3033–3044.
- (18) Chaudhary, A.; Pandeya, S. N.; Kumar, P.; Sharma, P. P.; Gupta, S.; Soni, N.; Verma, K. K.; Bhardwaj, G. Combretastatin a-4 analogs as anticancer agents. *Mini-Rev. Med. Chem.* **2007**, *7*, 1186–1205.
- (19) Shoichet, B. K. Virtual screening of chemical libraries. *Nature* **2004**, *432*, 862–865.
- (20) Schneider, G. Virtual screening: an endless staircase? *Nat. Rev. Drug Discovery* **2010**, *9*, 273–276.
- (21) Chiang, Y. K.; Kuo, C. C.; Wu, Y. S.; Chen, C. T.; Coumar, M. S.; Wu, J. S.; Hsieh, H. P.; Chang, C. Y.; Jseng, H. Y.; Wu, M. H.; Leou, J. S.; Song, J. S.; Chang, J. Y.; Lyu, P. C.; Chao, Y. S.; Wu, S. Y. Generation of ligand-based pharmacophore model and virtual screening for identification of novel tubulin inhibitors with potent anticancer activity. *J. Med. Chem.* **2009**, *52*, 4221–4233.
- (22) Kim, N. D.; Park, E. S.; Kim, Y. H.; Moon, S. K.; Lee, S. S.; Ahn, S. K.; Yu, D. Y.; No, K. T.; Kim, K. H. Structure-based virtual screening of novel tubulin inhibitors and their characterization as anti-mitotic agents. *Bioorg. Med. Chem.* **2010**, *18*, 7092–7100.
- (23) Nguyen, T. L.; McGrath, C.; Hermone, A. R.; Burnett, J. C.; Zaharevitz, D. W.; Day, B. W.; Wipf, P.; Hamel, E.; Gussio, R. A common pharmacophore for a diverse set of colchicine site inhibitors using a structure-based approach. *J. Med. Chem.* **2005**, *48*, 6107–6116.
- (24) Massarotti, A.; Theeramunkong, S.; Mesenzani, O.; Caldarelli, A.; Genazzani, A. A.; Tron, G. C. Identification of novel antitubulin agents by using a virtual screening approach based on a 7-point pharmacophore model of the tubulin colchi-site. *Chem. Biol. Drug Des.* **2011**, *78*, 913–922.
- (25) Dorleans, A.; Gigant, B.; Ravelli, R. B.; Mailliet, P.; Mikol, V.; Knossow, M. Variations in the colchicine-binding domain provide insight into the structural switch of tubulin. *Proc. Natl. Acad. Sci. U.S.A.* **2009**, *106*, 13775–13779.
- (26) Leynadier, D.; Peyrot, V.; Sarrazin, M.; Briand, C.; Andreu, J. M.; Rener, G. A.; Temple, C., Jr. Tubulin binding of two 1-deaza-7,8-dihydropteridines with different biological properties: enantiomers NSC 613862 (S)-(-) and NSC 613863 (R)-(+). *Biochemistry* **1993**, *32*, 10675–10682.
- (27) Bowdon, B. J.; Waud, W. R.; Wheeler, G. P.; Hain, R.; Dansby, L.; Temple, C., Jr. Comparison of 1,2-dihydropyrido[3,4-b]pyrazines (1-deaza-7,8-dihydropteridines) with several other inhibitors of mitosis. *Cancer Res.* **1987**, *47*, 1621–1626.
- (28) de Ines, C.; Leynadier, D.; Barasoain, I.; Peyrot, V.; Garcia, P.; Briand, C.; Rener, G. A.; Temple, C., Jr. Inhibition of microtubules and cell cycle arrest by a new 1-deaza-7,8-dihydropteridine antitumor drug, CI 980, and by its chiral isomer, NSC 613863. *Cancer Res.* **1994**, *54*, 75–84.
- (29) Kim, D. Y.; Kim, K.-H.; Kim, N. D.; Lee, K. Y.; Han, C. K.; Yoon, J. H.; Moon, S. K.; Lee, S. S.; Seong, B. L. Design and biological evaluation of novel tubulin inhibitors as antimitotic agents using a pharmacophore binding model with tubulin. *J. Med. Chem.* **2006**, *49*, 5664–5670.
- (30) Ravelli, R. B.; Gigant, B.; Curmi, P. A.; Jourdain, I.; Lachkar, S.; Sobel, A.; Knossow, M. Insight into tubulin regulation from a complex with colchicine and a stathmin-like domain. *Nature* **2004**, *428*, 198–202.
- (31) Meng, E. C.; Shoichet, B. K.; Kuntz, I. D. Automated docking with grid-based energy evaluation. *J. Comput. Chem.* **1992**, *13*, 505–524.
- (32) Lorber, D. M.; Shoichet, B. K. Hierarchical docking of databases of multiple ligand conformations. *Curr. Top. Med. Chem.* **2005**, *5*, 739–749.

- (33) Wei, B. Q.; Baase, W. A.; Weaver, L. H.; Matthews, B. W.; Shoichet, B. K. A model binding site for testing scoring functions in molecular docking. *J. Mol. Biol.* **2002**, *322*, 339–355.
- (34) Jacobson, M. P.; Kaminski, G. A.; Friesner, R. A.; Rapp, C. S. Force field validation using protein side chain prediction. *J. Phys. Chem. B* **2002**, *106*, 11673–11680.
- (35) Jacobson, M. P.; Pincus, D. L.; Rapp, C. S.; Day, T. J.; Honig, B.; Shaw, D. E.; Friesner, R. A. A hierarchical approach to all-atom protein loop prediction. *Proteins* **2004**, *55*, 351–367.
- (36) Li, X.; Jacobson, M. P.; Friesner, R. A. High-resolution prediction of protein helix positions and orientations. *Proteins* **2004**, *55*, 368–382.
- (37) Huang, N.; Kalyanaraman, C.; Irwin, J. J.; Jacobson, M. P. Physics-based scoring of protein-ligand complexes: enrichment of known inhibitors in large-scale virtual screening. *J. Chem. Inf. Model.* **2006**, *46*, 243–253.
- (38) Srinivasan, J.; Miller, J.; Kollman, P. A.; Case, D. A. Continuum solvent studies of the stability of RNA hairpin loops and helices. *J. Biomol. Struct. Dyn.* **1998**, *16*, 671–682.
- (39) Flynn, B. L.; Flynn, G. P.; Hamel, E.; Jung, M. K. The synthesis and tubulin binding activity of thiophene-based analogues of combretastatin A-4. *Bioorg. Med. Chem. Lett.* **2001**, *11*, 2341–2343.
- (40) Romagnoli, R.; Baraldi, P. G.; Cruz-Lopez, O.; Tolomeo, M.; Di Cristina, A.; Pipitone, R. M.; Grimaudo, S.; Balzarini, J.; Brancale, A.; Hamel, E. Synthesis of novel antimitotic agents based on 2-amino-3-aryloyl-5-(hetero)arylethyanyl thiophene derivatives. *Bioorg. Med. Chem. Lett.* **2011**, *21*, 2746–2751.
- (41) Romagnoli, R.; Baraldi, P. G.; Cara, C. L.; Hamel, E.; Basso, G.; Bertolozzi, R.; Viola, G. Synthesis and biological evaluation of 2-(3',4',5'-trimethoxybenzoyl)-3-aryl/arylaminobenzo[b]thiophene derivatives as a novel class of antiproliferative agents. *Eur. J. Med. Chem.* **2010**, *45*, 5781–5791.
- (42) Romagnoli, R.; Baraldi, P. G.; Pavani, M. G.; Cruz-Lopez, O.; Hamel, E.; Balzarini, J.; Brognara, E.; Zuccato, C.; Gambari, R. Synthesis and cellular pharmacology studies of a series of 2-amino-3-aryloyl-4-substituted thiophene derivatives. *Med. Chem.* **2010**, *6*, 329–343.
- (43) Liao, S. Y.; Chen, T. J.; Miao, T. F.; Qian, L.; Zheng, K. C. Binding orientations, QSAR, and molecular design of thiophene derivative inhibitors. *Chem. Biol. Drug Des.* **2009**, *74*, 289–296.
- (44) McGovern, S. L.; Helfand, B. T.; Feng, B.; Shoichet, B. K. A specific mechanism of nonspecific inhibition. *J. Med. Chem.* **2003**, *46*, 4265–4272.
- (45) Hsieh, J. H.; Yin, S.; Liu, S.; Sedykh, A.; Dokholyan, N. V.; Tropsha, A. Combined application of cheminformatics- and physical force field-based scoring functions improves binding affinity prediction for CSAR data sets. *J. Chem. Inf. Model.* **2011**, *51*, 2027–2035.
- (46) Hsieh, J. H.; Yin, S.; Wang, X. S.; Liu, S.; Dokholyan, N. V.; Tropsha, A. Cheminformatics meets molecular mechanics: a combined application of knowledge-based pose scoring and physical force field-based hit scoring functions improves the accuracy of structure-based virtual screening. *J. Chem. Inf. Model.* **2012**, *52*, 16–28.
- (47) Ducki, S. The development of chalcones as promising anticancer agents. *IDrugs* **2007**, *10*, 42–46.
- (48) Kuntz, I. D.; Chen, K.; Sharp, K. A.; Kollman, P. A. The maximal affinity of ligands. *Proc. Natl. Acad. Sci. U.S.A.* **1999**, *96*, 9997–10002.
- (49) Hopkins, A. L.; Groom, C. R.; Alex, A. Ligand efficiency: a useful metric for lead selection. *Drug Discovery Today* **2004**, *9*, 430–431.
- (50) Irwin, J. J.; Shoichet, B. K. ZINC—a free database of commercially available compounds for virtual screening. *J. Chem. Inf. Model.* **2005**, *45*, 177–182.
- (51) Connolly, M. L. Solvent-accessible surfaces of proteins and nucleic acids. *Science* **1983**, *221*, 709–713.
- (52) Ferrin, T. E.; Huang, C. C.; Jarvis, L. E.; Langridge, R. The MIDAS display system. *J. Mol. Graphics Modell.* **1988**, *6*, 13–27.
- (53) Kuntz, I. D.; Blaney, J. M.; Oatley, S. J.; Langridge, R.; Ferrin, T. E. A geometric approach to macromolecule-ligand interactions. *J. Mol. Biol.* **1982**, *161*, 269–288.
- (54) Nicholls, A.; Honig, B. A rapid finite difference algorithm, utilizing successive over-relaxation to solve the Poisson–Boltzmann equation. *J. Comput. Chem.* **1991**, *12*, 435–445.
- (55) Mysinger, M. M.; Shoichet, B. K. Rapid context-dependent ligand desolvation in molecular docking. *J. Chem. Inf. Model.* **2010**, *50*, 1561–1573.
- (56) Huang, N.; Kalyanaraman, C.; Bernacki, K.; Jacobson, M. P. Molecular mechanics methods for predicting protein-ligand binding. *Phys. Chem. Chem. Phys.* **2006**, *8*, 5166–5177.
- (57) Huang, N.; Jacobson, M. P. Binding-site assessment by virtual fragment screening. *PLoS One* **2010**, *5*, e10109.
- (58) Jorgensen, W. L.; Maxwell, D. S.; Tirado-Rives, J. Development and testing of the OPLS all-atom force field on conformational energetics and properties of organic liquids. *J. Am. Chem. Soc.* **1996**, *118*, 11225–11236.
- (59) Kaminski, G. A.; Friesner, R. A.; Tirado-Rives, J.; Jorgensen, W. L. Evaluation and reparametrization of the OPLS-AA force field for proteins via comparison with accurate quantum chemical calculations on peptides? *J. Phys. Chem. B* **2001**, *105*, 6474–6487.
- (60) Case, D. A.; Darden, T. A.; Cheatham, I. T. E.; Simmerling, C. L.; Wang, J.; Duke, R. E.; Luo, R.; Crowley, M.; Walker, R. C.; Zhang, W.; Merz, K. M.; Wang, B.; Hayik, S.; Roitberg, A.; Seabra, G.; Kolossváry, I.; Wong, K. F.; Paesani, F.; Vanicek, J.; Wu, X.; Brozell, S. R.; Steinbrecher, T.; Gohlke, H. *AMBER 10*; University of California: San Francisco, CA, 2008.
- (61) Wang, J.; Cieplak, P.; Kollman, P. A. How well does a restrained electrostatic potential (RESP) model perform in calculating conformational energies of organic and biological molecules? *J. Comput. Chem.* **2000**, *21*, 1049–1074.
- (62) Wang, J.; Wolf, R. M.; Caldwell, J. W.; Kollman, P. A.; Case, D. A. Development and testing of a general amber force field. *J. Comput. Chem.* **2004**, *25*, 1157–1174.
- (63) Luo, R.; David, L.; Gilson, M. K. Accelerated Poisson–Boltzmann calculations for static and dynamic systems. *J. Comput. Chem.* **2002**, *23*, 1244–1253.
- (64) Sitkoff, D.; Sharp, K. A.; Honig, B. Accurate calculation of hydration free energies using macroscopic solvent models. *J. Phys. Chem.* **1994**, *98*, 1978–1988.
- (65) Castoldi, M.; Popov, A. V. Purification of brain tubulin through two cycles of polymerization-depolymerization in a high-molarity buffer. *Protein Expression Purif.* **2003**, *32*, 83–88.
- (66) Shan, B.; Medina, J. C.; Santha, E.; Frankmoelle, W. P.; Chou, T. C.; Learned, R. M.; Narbut, M. R.; Stott, D.; Wu, P.; Jaen, J. C.; Rosen, T.; Timmermans, P. B.; Beckmann, H. Selective, covalent modification of beta-tubulin residue Cys-239 by T138067, an antitumor agent with in vivo efficacy against multidrug-resistant tumors. *Proc. Natl. Acad. Sci. U.S.A.* **1999**, *96*, 5686–5691.